Journal of Power Sources 185 (2008) 1420–1424

Contents lists available at ScienceDirect

Journal of Power Sources

journal homepage: www.elsevier.com/locate/jpowsour

Short communication

Electrochemical fabrication of anatase TiO_2 nanostructure as an anode material for aqueous lithium-ion batteries

Mao-Sung Wu[a,*], Min-Jyle Wang[a], Jiin-Jiang Jow[a], Wein-Duo Yang[a], Ching-Yuan Hsieh[b], Huei-Mei Tsai[b]

[a] Department of Chemical and Materials Engineering, National Kaohsiung University of Applied Sciences, 415 Chien Kung Road, Kaohsiung 807, Taiwan, ROC
[b] Materials & Electro-Optics Research Division, Battery Section, Chung-Shan Institute of Science & Technology, Lung-Tan, Tao-Yuan 325, Taiwan, ROC

ARTICLE INFO

Article history:
Received 5 August 2008
Received in revised form 3 September 2008
Accepted 10 September 2008
Available online 18 September 2008

Keywords:
Titanium oxide
Lithium-ion storage
Intercalated compound
Nanostructured materials
Aqueous lithium-ion batteries

ABSTRACT

Nanostructured titanium oxide films are fabricated directly by an anodic electrodeposition strategy at an aqueous $TiCl_3$ solution. Surface morphology shows that the deposited films are consisted of fine particles having 15–25 nm in diameter. Annealing temperature influences both the crystal structure and the electrochemical performance of the deposited titanium oxide. When the annealing temperature exceeds 300 °C, the poorly crystalline titanium oxide converts into anatase phase. Cyclic voltammograms (CVs) show that the anatase titanium oxide films exhibit reversible insertion/de-insertion of lithium ion in an aqueous LiOH electrolyte. The formation of lithiated titanium oxide is confirmed from an X-ray photoelectron spectroscopy. An optimal annealing temperature is found to be about 400 °C in terms of the CV peak current density. In addition, the diffusion coefficient of lithium ion in cathodic process (1.6×10^{-15} cm^2 s^{-1}) is higher than that of anodic process (9.4×10^{-16} cm^2 s^{-1}), probably due to the formation of higher O–Li bond strength during the lithium insertion.

1. Introduction

Demand on rechargeable batteries for portable electronics has become pressing. While these electronics tend to decrease in size and become thin, batteries of variable sizes and shapes must consequently evolve to compensate these new requirements. Among many rechargeable batteries, lithium-ion battery is most attractive because of its high energy density, high working voltage, and low self-discharge rate. Most of the researches on lithium-ion batteries are focused on the non-aqueous electrolyte.

Recently, Li et al. [1–3] have proposed a new type of rechargeable lithium batteries with aqueous electrolyte. Aqueous lithium-ion battery is one of the promising candidates for energy storage in terms of safety and cost. More recently, Wang et al. [4–6] have proposed a hybrid aqueous energy-storage cell using $LiMn_2O_4$, $LiCoO_2$, and $LiCo_{1/3}Ni_{1/3}Mn_{1/3}O_2$ as the positive electrode and activated carbon as the negative electrode. In addition, MnO_2, $LiMnPO_4$, and $LiFePO_4$ cathode materials for lithium-ion storage in aqueous electrolyte were also reported [7–11].

It has reported that electrodes made of nanoparticles of metal oxides (MO, where M is Co, Ni, Mn, Cu or Fe) demonstrate high electrochemical capacities (about 700 mAh g^{-1}), great capacity retention, and high discharging rates in non-aqueous electrolyte [12–18]. However, lithium insertion materials as the anode materials for aqueous lithium-ion batteries are rarely studied earlier. Titanium oxides especially in anatase phase have reported to be the anode materials for lithium-ion insertion/de-insertion in an aqueous LiOH electrolyte [19,20].

Recently, much effort has been directed toward the fabrication of nanostructured titanium oxides because of their potential applications in photocatalysts, dye-sensitized solar cells, and non-aqueous lithium-ion batteries, etc. [21–40]. Most of these useful functions depend mainly on the composition, configuration, and structure. Nanostructured titanium oxides are believed to have better properties than those of their bulk counterparts. It is generally believed that nanostructured materials play an important role in electrochemical performance because high-specific surface area and short diffusion path enhance electrochemical behavior of the applied battery. Generally, lithium-ion diffusion within the crystal structure of active material dominates the high-rate charging and discharging of the electrode. Diffusion resistance of lithium ions within the material can be decreased by shortening the diffusion path; therefore, nanostructure is advantageous in improving the high-rate performances of materials.

To the best of our knowledge, the anodically electrodeposited anatase titanium oxide for aqueous lithium-ion batteries has not

* Corresponding author. Fax: +886 9 45614423.
E-mail address: ms_wu@url.com.tw (M.-S. Wu).

0378-7753/$ – see front matter © 2008 Elsevier B.V. All rights reserved.
doi:10.1016/j.jpowsour.2008.09.017

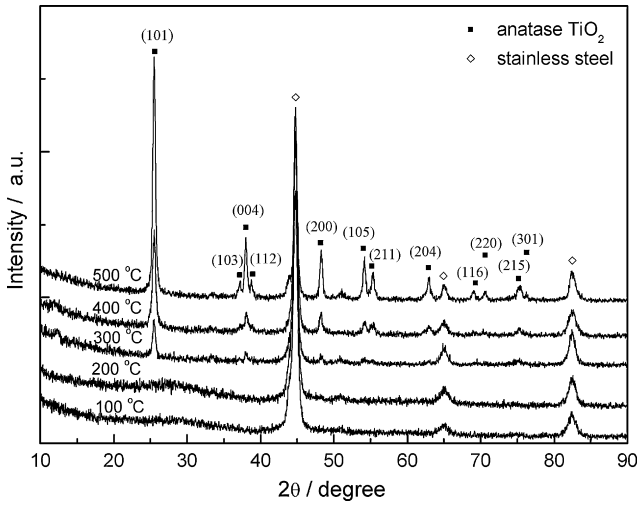

Fig. 1. XRD patterns of the deposited titanium oxide films after annealing at various temperatures.

been reported earlier. Therefore, in this work, the electrochemically anodic deposition strategy is used to fabricate the anatase titanium oxide films directly onto the stainless steel substrate at room temperature. In addition, electrochemical performance of the synthesized titanium oxide film after annealing at different temperatures is also investigated in an aqueous LiOH electrolyte.

2. Experimental

Titanium oxide films were deposited directly on both sides of the stainless steel (SS) foil (2 cm × 2 cm) by applying an anodic current density of 0.15 mA cm^{-2}. The plating solution consisted of 0.25 M $TiCl_3$ solution at room temperature under a nitrogen atmosphere [25,40–43]. The plating solution of pH 2.5 was stirred by a Teflon stir bar on a magnetic hot plate during the entire deposition. The pH value of the plating solution was adjusted by Na_2CO_3 solution. Prior to electrochemical deposition, SS foils were polished with emery paper and rinsed by ultrasonic vibrations in acetone and de-ionized water, respectively. After deposition, films were rinsed several times in de-ionized water and then dried for 3 h in air at 100, 200, 300, 400, and 500 °C, respectively. The amount of deposited films was measured by a microbalance (Ohaus G160, USA) with an accuracy of 0.01 mg and was held almost the same (about 0.5 mg) for each deposited film by adjusting the deposition time. The deposition time for the film deposited at 0.15 mA cm^{-2} was around 20 min. Note that all electrochemical experiments were carried out in a three-compartment cell. A saturated calomel electrode (SCE) was used as the reference electrode

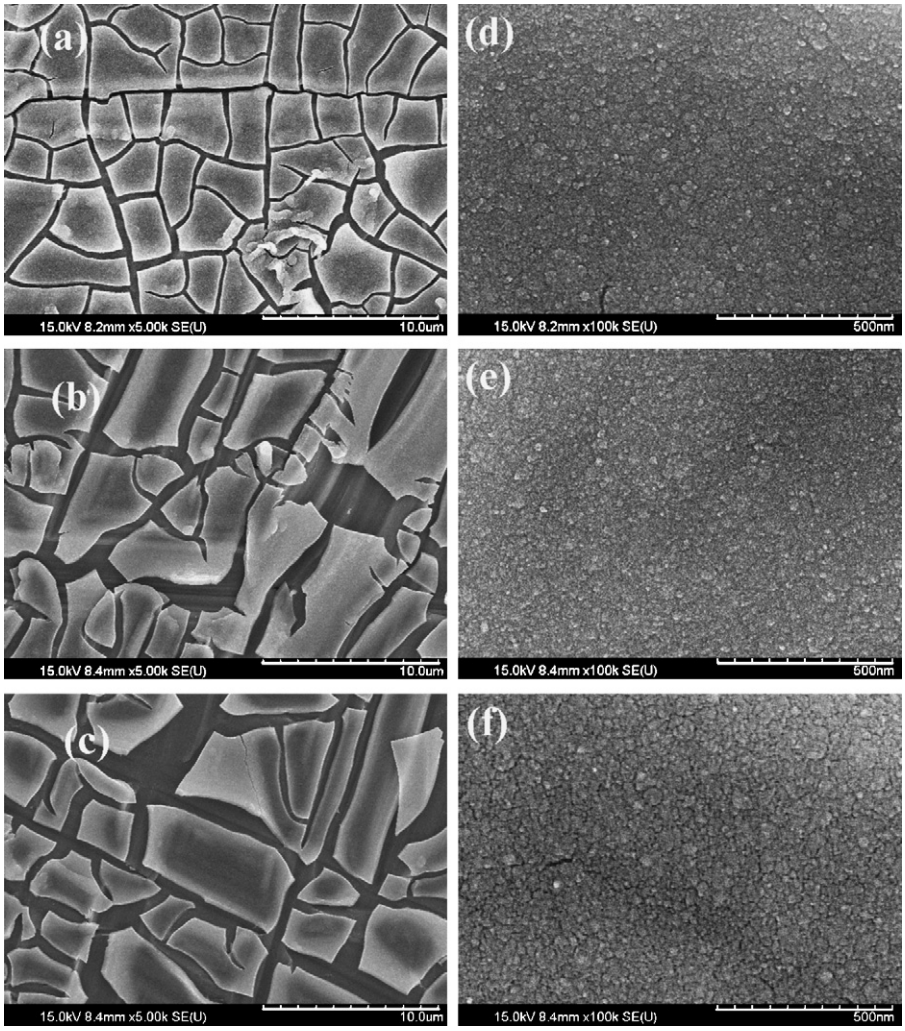

Fig. 2. SEM micrographs of the titanium oxide films after annealing at: (a) 100 °C, (b) 300 °C, and (c) 500 °C, respectively. High magnification images of (a), (b), and (c) are shown in (d), (e), and (f), respectively.

and a platinum foil with dimension 2 cm × 2 cm was the counter electrode.

Electrochemical characteristics of the deposited films were determined by cyclic voltammetry in a three-electrode cell with 1 M LiOH electrolyte. The potential was cycled at different scan rates using a potentiostat (CH Instruments CHI 608, USA) in a range of 0.1 to −1.3 V. Surface morphology of the deposited films was examined with a field-emission electron microscope (FE-SEM, Jeol JEOL-6330, USA) with an accelerating voltage of 15 keV. Crystal structure of the deposited films was identified by a glance angle X-ray diffractometer (GAXRD, Rigaku D/MAX2500, Japan) with a Cu Kα target (wavelength = 1.54056 Å) and an incidence angle of 2°. Diffraction data were collected for 1 s at each 0.04° step width over 2θ, ranging from 10° to 90°. In addition, an X-ray photoelectron spectroscopy (Perkin Elmer PHI Quantera SXM, USA) with a focused monochromatic Al Kα radiation (1486.6 eV) was used to analyze the composition of the deposited titanium oxide films before and after the electrochemical insertion of lithium.

3. Results and discussion

Fig. 1 shows XRD patterns of the deposited titanium oxide films after annealing at various temperatures. When the annealing temperature is lower than 300 °C, in addition to the diffraction peaks of the SS substrate, there is no detectable peak of the titanium oxide indicating that the deposited titanium oxide film is poorly crystalline structure. Clearly, some characteristic peaks of the anatase TiO_2 (JCPDS 89-4921) appear, when the deposited film is annealed at a temperature higher than 300 °C, suggesting that the poorly crystalline (nanocrystalline) titanium oxide partially converts into anatase phase. As evident from Fig. 1, the XRD peak at about $2\theta = 25.4°$ becomes broader as the annealing temperature decreases from 500 to 300 °C; such a widening indicates a poor crystallinity and a decrease of the average grain size by the decrease in annealing temperature. The mean grain size of the anatase TiO_2 was calculated using Scherrer's equation with diffraction peak at $2\theta = 25.4°$, $D = 0.9\lambda/(\beta \cos\theta)$, where λ is the X-ray wavelength (1.54056 Å), β is the full width at half maximum (FWHM), and θ is the Bragg angle. The calculated grain sizes at 300, 400, and 500 °C are 15, 18, and 22 nm, respectively.

Fig. 2 shows SEM micrographs of the titanium oxide films after different annealing temperatures. After annealing at 100 °C for 1 h, there are many crevices with submicron meter formed on the deposited titanium oxide film, possibly due to the removal of hydrated water during drying process. These crevices are enlarged widthwise by increasing the annealing temperature. It was reported that only a small percentage of water in the electrodeposited manganese dioxide is volatile at 120 °C, and a predominant portion of water is desorbed in a relatively smooth manner up to 350 °C [44]. Therefore, the change in surface morphology after higher temperature annealing may be attributed to the removal of both the surface and the structural water from the solid phase of titanium oxide structure. In addition, the phase transition of titanium oxide from poorly crystalline phase to anatase phase during annealing may also induce stress variation resulting in crevices. Possibly, theses crevices are in favor of electrolyte penetration resulting in a better electrochemical performance. Inspection of high magnification morphology (Fig. 2d) shows that the deposited titanium oxide film after annealing at 100 °C is composed of fine particles having 15–25 nm in diameter; in addition, the surface morphology is not greatly affected by the annealing temperature ranging from 100 to 500 °C (Fig. 2d–f).

Fig. 3a shows CV curves of the titanium oxide films after annealing at different temperatures. There is no significant redox peak for

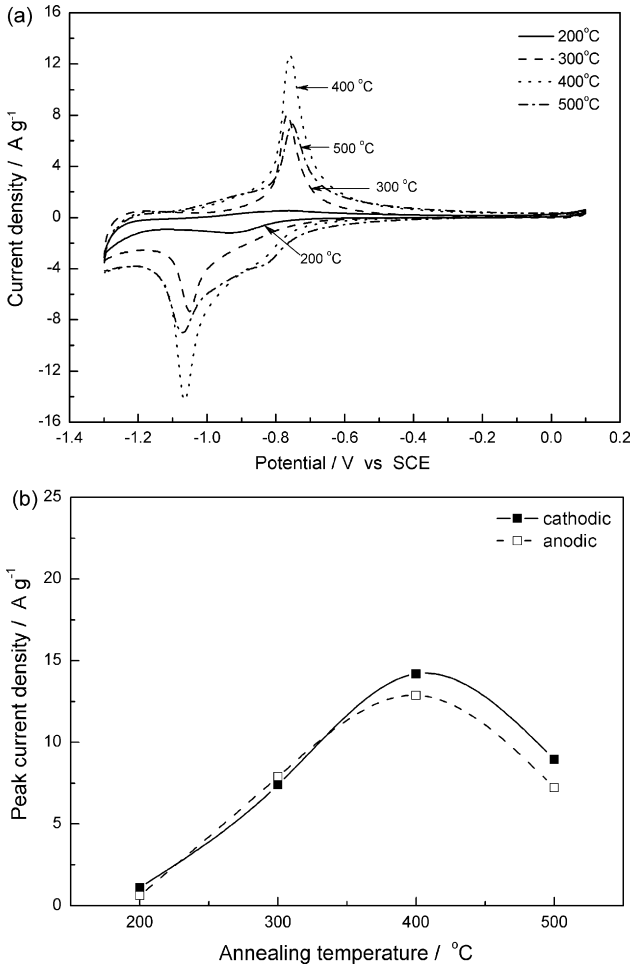

Fig. 3. (a) CV curves of the titanium oxide films after annealing at different temperatures and (b) relationship between peak current density and annealing temperature. Scan rate: 25 mV s^{-1}.

the film annealed at temperature below 300 °C suggesting that the titanium oxide film with poorly crystalline phase blocks the electrochemical reactions. Interestingly, when the annealing temperature is higher than 300 °C, the titanium oxide film (anatase phase) shows a redox couple during CV scan; a cathodic peak at about −1.06 V vs. SCE in the cathodic process, and an anodic peak at −0.82 V vs. SCE in the anodic process. These two peaks might be attributed by the reversible electrochemical oxidation and reduction of the anatase titanium oxide with lithium ion in an aqueous lithium hydroxide solution. The lithium-ion insertion/de-insertion process in anatase titanium oxide can be written as follows:

$$TiO_2 + xLi^+ + xe^- \leftrightarrow Li_xTiO_2 \quad (1)$$

Peak current density of the deposited films after annealing at different temperatures is shown in Fig. 3b. The peak current density increases with elevating the annealing temperature, it reaches a maximum at 400 °C and then decreases with further increase in the annealing temperature. This finding suggests that the titanium oxide with anatase phase favors lithium insertion and de-insertion. The higher the annealing temperature, the higher the degree of crystallinity of the anatase titanium oxide, therefore the peak current density is enhanced by the annealing temperature in a range of 200–400 °C. When the annealing is higher than 400 °C, the peak current density decreases due to the increased grain size of the anatase titanium oxide by elevating temperature. It is believed that the peak current density is dominated by the mass-transfer resis-

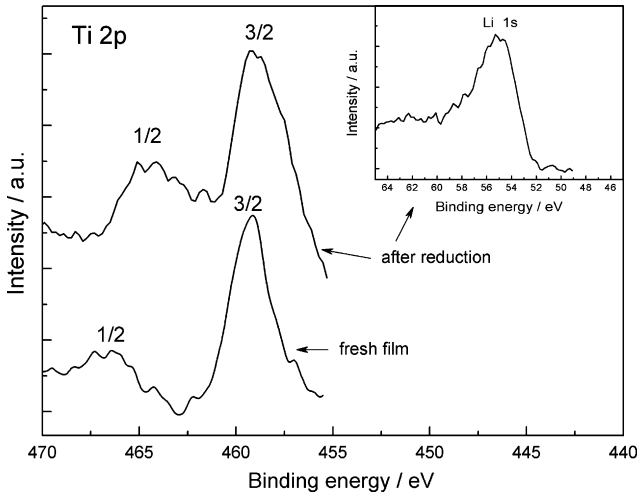

Fig. 4. XPS spectra of the anatase titanium oxide films before and after electrochemical reduction.

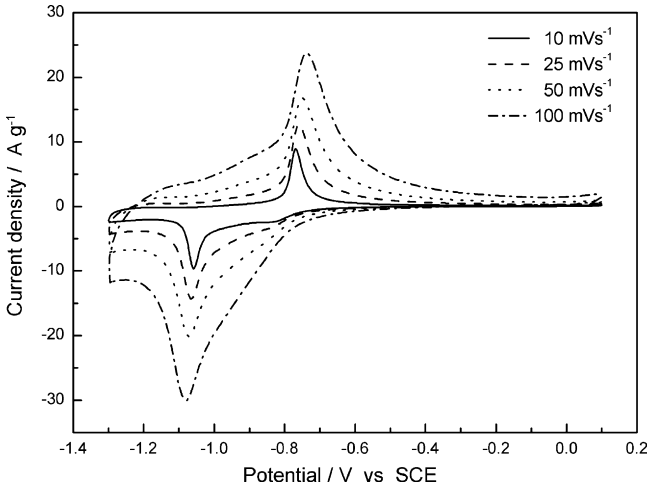

Fig. 6. CV curves of the anatase titanium oxide film at different scan rates. Prior to electrochemical measurements, film was annealed at 400 °C for 1 h.

tance of lithium ions within the solid-state material rather than the electrolyte, therefore increasing the grain size is detrimental to the solid-state diffusion of the lithium ions.

Fig. 4 shows XPS spectra of the anatase titanium oxide films before and after electrochemical reduction (insertion). Prior to electrochemical experiments, the titanium oxide film was annealed at 400 °C for 1 h. Before electrochemical reduction, the two significant peaks of binding energies correspond to Ti $2p_{1/2}$ and Ti $2p_{3/2}$, respectively, which identify the major chemical composition being TiO_2. In order to further understand the electrochemical mechanism of the reactions between anatase titanium oxide and lithium ion, XPS measurement has been applied to investigate the valence change of titanium after the lithium-ion insertion as shown in Fig. 4. Prior to XPS measurements, the anatase titanium oxide electrode has been charged to −1.3 V vs. SCE. Clearly, the two significant peaks of binding energies, corresponding to Ti $2p_{1/2}$ and Ti $2p_{3/2}$, respectively, shift to lower binding energy. This chemical shift reflects the change of Ti^{4+} to Ti^{3+} oxidation state indicating the formation of lithium intercalated titanium oxide phase (Li_xTiO_2) [19]. The Li 1s XPS spectrum for the anatase titanium oxide electrode after electrochemical reduction is also presented in the insert of Fig. 4. The binding energy peak of 55.3 eV assigned to Li 1s attributes to the lithium-ion insertion into the anatase titanium oxide by Eq. (1). Similar results were found in a commercial anatase TiO_2 electrode in an aqueous lithium hydroxide electrolyte [19].

Fig. 5 shows XRD diffraction patterns of the titanium oxide films before and after electrochemical reduction. Clearly, in addition to the diffraction peaks of the anatase titanium oxide and the SS substrate, some characteristic peaks of lithiated titanium oxides, Li_xTiO_2 (JCPDS 51-0050) and $Li_{0.5}TiO_2$ (JCPDS 51-0049), appear. This confirms that after electrochemical reduction, the lithium ion inserts into the anatase titanium oxide leading to the formation of lithiated titanium oxide (Li_xTiO_2 and $Li_{0.5}TiO_2$). It was reported that since the ionic radius of lithium ion is almost identical to that of Ti^{3+}, the formation of lithium intercalated titanium oxide is reasonable [19]. In addition, the electrochemical behavior of deposited anatase titanium oxide in aqueous LiOH electrolyte is similar to that of non-aqueous $LiClO_4$ electrolyte [26].

Fig. 6 shows CV curves of the anatase titanium oxide film at different scan rates. Prior to CV scan, the film was annealed at 400 °C for 1 h. Clearly, the intensity of reduction and oxidation peak currents gradually increases with increasing the scan rate. Fig. 7 shows linear relationship between the peak current and the square root of scan rate in cathodic and anodic processes, respectively. The linearity suggests a diffusion-limited reaction (semi-infinite diffu-

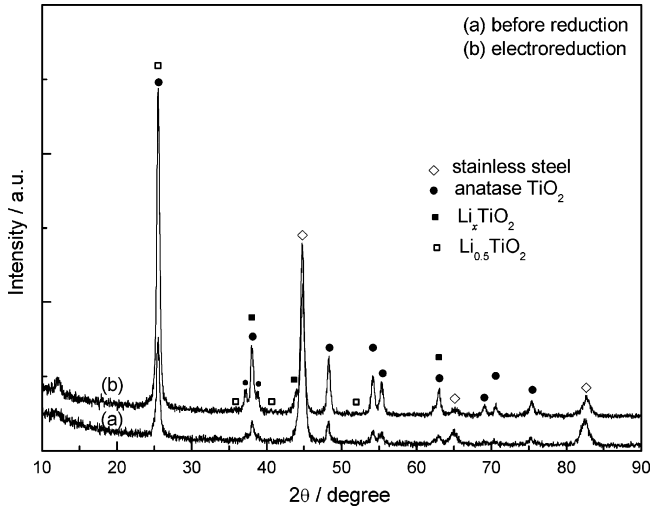

Fig. 5. XRD patterns of the titanium oxide films before and after electrochemical reduction.

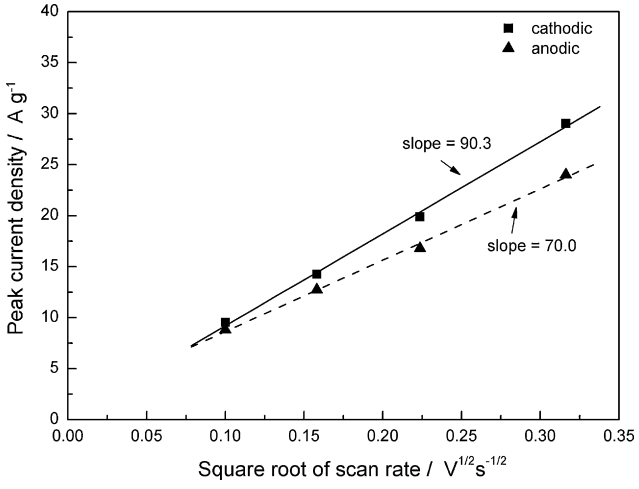

Fig. 7. Relationship between the peak current density and the square root of scan rate in cathodic and anodic processes.

sion). The peak current density i_p may be expressed by the classical Randles–Sevick equation at 25 °C [45]:

$$i_p = (2.69 \times 10^5) n^{3/2} C_o A D^{1/2} v^{1/2} \quad (2)$$

where n is the number of electrons transferred, i_p is the current density ($A\,g^{-1}$), D ($cm^2\,s^{-1}$) is the diffusion coefficient of the rate limiting species (lithium ion), A is apparent surface area ($cm^2\,g^{-1}$), v is the scan rate ($V\,s^{-1}$), and C_o ($mol\,cm^{-3}$) is the maximum lithium concentration ($C_o = 0.024\,mol\,cm^{-3}$ for $x = 0.5$) [38]. By fitting the slope of i_p vs. $v^{1/2}$ in Fig. 7 into Eq. (2), lithium diffusion coefficient in the nanostructured anatase titanium oxide during cathodic and anodic processes can be estimated. Clearly, the slope of Eq. (2) in cathodic process (lithium insertion) is higher than that of anodic process reflecting that the diffusion coefficient of lithium insertion is higher than that of lithium de-insertion. This finding suggests that as the anatase titanium oxide is inserted as O–Li bond, the higher O–Li bond strength makes the lithium de-insertion slow, which lowers the diffusivity of lithium ion within titanium oxide. Van De Krol et al. [46] indicated that the striking difference between lithium insertion and de-insertion coefficients can be explained by the number of unoccupied octahedral sites per unit cell available for lithium-ion transport, which is four for TiO_2 vs. two for $Li_{0.5}TiO_2$. Lithium diffusion coefficient is estimated to be about $1.6 \times 10^{-15}\,cm^2\,s^{-1}$ for insertion and $9.4 \times 10^{-16}\,cm^2\,s^{-1}$ for de-insertion; the apparent surface area is assumed $100\,m^2\,g^{-1}$. These diffusion coefficients compare well with those reported for surfactant-templated anatase TiO_2 in aprotic electrolyte [38].

4. Conclusions

Nanostructured titanium oxide films are successfully deposited onto the SS substrate from simple aqueous titanium chloride solution by an anodic electrodeposition strategy. The XRD results show that the poorly crystalline titanium oxide converts into anatase phase, when the annealing temperature exceeds 300 °C. Annealing temperature affects not only the crystal structure of deposited titanium oxide, but also the electrochemical performance in an aqueous LiOH electrolyte. The higher the annealing temperature, the higher the degree of crystallinity. The CV results show that the poorly crystalline titanium oxide film exhibits poor electrochemical performance in lithium insertion/de-insertion, while the anatase titanium oxide films show reversible CV indicating that the lithium-ion insertion/de-insertion occurs reversibly. The lithium-ion insertion into the host titanium oxide material (anatase phase) in an aqueous LiOH solution is evident from the shift of binding energies of Ti $2p_{1/2}$ and Ti $2p_{3/2}$ in XPS. This chemical shift reflects the change of Ti^{4+} to Ti^{3+} oxidation state indicating the formation of lithiated titanium oxide phase (Li_xTiO_2). In addition, a binding energy peak of 55.3 eV, which assigns to Li 1s, is attributed to the lithium-ion insertion into the anatase titanium oxide. An optimal annealing temperature of 400 °C is found in terms of the peak current density during CV scan. When the annealing is higher than 400 °C, the peak current density decreases due to the increased grain size of the anatase titanium oxide by elevating the annealing temperature. Diffusion coefficient of the lithium insertion is higher than that of lithium de-insertion due to the formation of higher O–Li bond strength in the lithium insertion process.

Acknowledgement

The authors gratefully acknowledge a financial support from the National Science Council, Taiwan, ROC (Project No.: NSC 97-2221-E-151-029).

References

[1] W. Li, J.R. Dahn, D.S. Wainwright, Science 264 (1994) 1115.
[2] W. Li, W.R. Mckinnon, J.R. Dahn, J. Electrochem. Soc. 141 (1994) 2310.
[3] W. Li, J.R. Dahn, J. Electrochem. Soc. 142 (1995) 1742.
[4] Y.G. Wang, Y.Y. Xia, J. Electrochem. Soc. 153 (2006) A450.
[5] Y.G. Wang, J.Y. Luo, C.X. Wang, Y.Y. Xia, J. Electrochem. Soc. 153 (2006) A1425.
[6] Y.G. Wang, J.Y. Luo, W. Wu, C.X. Wang, Y.Y. Xia, J. Electrochem. Soc. 154 (2007) A228.
[7] M.S. Wu, R.H. Lee, J. Power Sources 176 (2008) 363.
[8] M. Manickam, P. Singh, T.B. Issa, S. Thurgate, R.D. Macro, J. Power Sources 130 (2004) 254.
[9] M. Manickam, P. Singh, D.R.G. Mitchell, J. Electrochem. Soc. 154 (2007) A109.
[10] M. Minakshi, P. Singh, S. Thurgate, K. Prince, Electrochem. Solid-State Lett. 9 (2006) A471.
[11] M. Minakshi, P. Singh, S. Thurgate, K. Prince, J. Power Sources 158 (2004) 646.
[12] P. Poizot, S. Laruelle, S. Grugeon, L. Dupont, J.-M. Tarascon, Nature 407 (2000) 496.
[13] Y. Wang, Y.F. Zhang, H.R. Liu, S.J. Yu, Q.Z. Qin, Electrochim. Acta 48 (2003) 4253.
[14] G.X. Wang, Y. Chen, K. Konstantinov, J. Yao, J. Ahn, H.K. Liu, S.X. Dou, J. Alloys Compd. 340 (2002) L5.
[15] Y.M. Kang, M.S. Song, J.H. Kim, H.S. Kim, M.S. Park, J.Y. Lee, H.K. Liu, S.X. Dou, Electrochim. Acta 50 (2005) 3667.
[16] J. Morales, L. Sanchez, S. Bijani, L. Martinez, M. Gabas, J.R. Ramos-Barrado, Electrochem. Solid-State Lett. 8 (2005) A159.
[17] M.S. Wu, P.C. Chiang, J.T. Lee, J.C. Lin, J. Phys. Chem. B 109 (2005) 23279.
[18] M.S. Wu, P.C. Chiang, Electrochem. Commun. 8 (2006) 383.
[19] M. Manickam, P. Singh, T.B. Issa, S. Thurgate, J. Appl. Electrochem. 36 (2006) 599.
[20] K.H. Reiman, K.M. Brace, T.J. Gordon-Smith, I. Nandhakumar, G.S. Attard, J.R. Owen, Electrochem. Commun. 8 (2006) 517.
[21] J. Nowotny, T. Bak, M.K. Nowotny, L.R. Sheppard, Int. J. Hydrogen Energy 32 (2007) 2609.
[22] Y.A. Shaban, S.U.M. Khan, Int. J. Hydrogen Energy 33 (2008) 1118.
[23] S. Kumari, Y.S. Chaudhary, S.A. Agnihotry, C. Tripathi, A. Verma, D. Chauhan, R. Shrivastav, S. Dass, V.R. Satsangi, Int. J. Hydrogen Energy 32 (2007) 1299.
[24] A. Manivannan, N. Spataru, K. Arihara, A. Fujishima, Electrochem. Solid-State Lett. 8 (2005) C138.
[25] K. Wessels, A. Feldhoff, M. Wark, J. Rathousky, T. Oekermann, Electrochem. Solid-State Lett. 9 (2006) C93.
[26] S. Karuppuchamy, M. Iwasaki, H. Minoura, Appl. Surf. Sci. 253 (2006) 2924.
[27] H. Yamada, T. Yamato, I. Moriguchi, T. Kudo, Solid State Ionics 175 (2004) 195.
[28] H. Furukawa, M. Hibino, I. Honma, J. Electrochem. Soc. 151 (2004) A527.
[29] Z. Bing, Y. Yuan, Y. Wang, Z.W. Fu, Electrochem. Solid-State Lett. 9 (2006) A101.
[30] R. Nakamura, A. Imanishi, K. Murakoshi, Y. Nakato, J. Am. Chem. Soc. 125 (2003) 7443.
[31] S. Yurdakal, G. Palmisano, V. Loddo, V. Augugliaro, L. Palmisano, J. Am. Chem. Soc. 130 (2008) 1568.
[32] E. Borgarello, J. Kiwi, E. Pelizzetti, M. Visca, M. Grätzel, Nature 289 (1981) 158.
[33] U. Bach, D. Lupo, P. Comte, J.E. Moser, F. Weissörtel, J. Salbeck, H. Spreitzer, M. Grätzel, Nature 395 (1998) 583.
[34] M. Grätzel, Nature 414 (2001) 338.
[35] B. O'Regan, M. Grätzel, Nature 353 (1991) 737.
[36] J.N. Clifford, E. Palomares, M.K. Nazeeruddin, R. Thampi, M. Grätzel, J.R. Durrant, J. Am. Chem. Soc. 126 (2004) 5670.
[37] M. Wagemaker, R. Van De Krol, A.P.M. Kentgens, A.A. Van Well, F.M. Mulder, J. Am. Chem. Soc. 123 (2001) 11454.
[38] L. Kavan, J. Rathousky, M. Grätzel, V. Shklover, A. Zukal, J. Phys. Chem. B 104 (2000) 12012.
[39] M. Zukalova, M. Kalbac, L. Kavan, I. Exnar, M. Grätzel, Chem. Mater. 17 (2005) 1248.
[40] L. Kavan, M. Zukalova, M. Kalbac, M. Grätzel, J. Electrochem. Soc. 151 (2004) A1301.
[41] M. Kalbac, O. Frank, L. Kavan, M. Zukalova, J. Prochazka, M. Klementova, L. Dunsch, J. Electrochem. Soc. 154 (2007) K19.
[42] L. Kavan, B. O'Regan, A. Kay, M. Grätzel, J. Electroanal. Chem. 346 (1993) 291.
[43] X. Zhang, B. Yao, L. Zhao, C. Liang, L. Zhang, Y. Mao, J. Electrochem. Soc. 148 (2001) G398.
[44] E. Preisler, J. Appl. Electrochem. 6 (1976) 311.
[45] Southampton Electrochemistry Group, Instrumental Methods in Electrochemistry, Ellis Horwood, England, 1985.
[46] R. Van De Krol, A. Goossens, J. Schoonman, J. Phys. Chem. B 103 (1999) 7151.